© 2019. Published by The Company of Biologists Ltd | Journal of Cell Science (2019) 132, jcs235531. doi:10.1242/jcs.235531

SHORT REPORT

Rap1 and membrane lipids cooperatively recruit talin to trigger integrin activation

Thomas Bromberger[1,*], Liang Zhu[2,*], Sarah Klapproth[1], Jun Qin[2,‡] and Markus Moser[1,3,‡]

ABSTRACT

Recruitment and tethering of talin to the plasma membrane initiate the process of integrin activation. Multiple factors including the Rap1 proteins, RIAM (also known as APBB1IP) and PIP_2 bind talin proteins and have been proposed to regulate these processes, but not systematically analyzed. By expressing specific talin mutants into talin-null fibroblasts, we show that binding of the talin F0 domain to Rap1 synergizes with membrane lipid binding of the talin F2 domain during talin membrane targeting and integrin activation, whereas the interaction of the talin rod with RIAM was dispensable. We also characterized a second Rap1-binding site within the talin F1 domain by detailed NMR analysis. Interestingly, while talin F1 exhibited significantly weaker Rap1-binding affinity than talin F0, expression of a talin F1 Rap1-binding mutant inhibited cell adhesion, spreading, talin recruitment and integrin activation similarly to the talin F0 Rap1-binding mutant. Moreover, the defects became significantly stronger when both Rap1-binding sites were mutated. In conclusion, our data suggest a model in which cooperative binding of Rap1 to the talin F0 and F1 domains synergizes with membrane PIP_2 binding to spatiotemporally position and activate talins to regulate integrin activity.

KEY WORDS: Integrin, Small GTPase, Rap1, Talin, RIAM, NMR

INTRODUCTION

Integrins are heterodimeric transmembrane receptors that mediate strong adhesion of cells to the extracellular matrix or other cells by connecting the extracellular ligand with the intracellular actin cytoskeleton. The formation of integrin adhesion complexes is either initiated by the extracellular ligand or by intracellular integrin activators such as talins that induce the conformational change of the integrin's extracellular domain towards a high affinity state for ligand binding.

Talin1 and talin2 are large (270 kDa) cytoplasmic adapter proteins consisting of an N-terminal 4.1 protein, ezrin, radixin, moesin (FERM)-like head domain, which binds the cytoplasmic domain of β integrin subunits, and a long C-terminal rod domain forming multiple connections with the actin cytoskeleton (Calderwood et al., 2013; Klapholz and Brown, 2017). In resting cells, a large portion of talin proteins (talin hereafter) reside in the cytoplasm in a closed, auto-inhibited conformation (Banno et al., 2012; Goult et al., 2013), in which intramolecular interactions between the head and rod domains prevent integrin binding (Goksoy et al., 2008; Goult et al., 2009; Zhang et al., 2016). Upon stimulation, talin is efficiently recruited to the plasma membrane and released from its auto-inhibitory conformation to trigger integrin activation. However, the molecular mechanisms behind these crucial events are not fully understood.

Previous studies have suggested that talin-mediated integrin activation is highly dependent on the membrane-anchored small GTPase Rap1 protein family (Bos, 2005; Caron et al., 2000; Katagiri et al., 2000; Reedquist et al., 2000; Sebzda et al., 2002; Han et al., 2006). One model has suggested that talin membrane recruitment is triggered via the Rap1 effector RIAM (also known as APBB1IP), which binds the talin rod domain and thereby links it to the plasma membrane (Lagarrigue et al., 2016; Lee et al., 2009). However, this Rap1–RIAM–talin pathway is only crucial for leukocyte β2 integrin activation, but dispensable for integrin regulation in other cells such as platelets (Klapproth et al., 2015; Stritt et al., 2015; Su et al., 2015). We recently identified a direct 'Rap1–talin' membrane targeting pathway to regulate integrin activity in mammals, which was previously observed in *Dictyostelium discoideum* (Plak et al., 2016; Zhu et al., 2017). The physiological relevance of this pathway was subsequently demonstrated in mice and flies by us and others (Bromberger et al., 2018; Camp et al., 2018). However, while mutant flies that are deficient in Rab1 binding show embryonic lethality, a phenotype resembling that of talin-null mutants (Brown et al., 2002), Rap1-binding mutant mice comprising a talin knockin showed rather mild integrin defects in leukocytes and platelets (Bromberger et al., 2018). In particular, the weak platelet phenotype, when compared to that of mice in which both genes encoding Rap1 proteins (*Rap1a*/*b*) or *talin1* were genetically deleted in platelets (Nieswandt et al., 2007; Stefanini et al., 2018), suggests that the interaction mode between talin and Rap1 proteins (Rap1 hereafter) is more complex in mammals. Consistent with this assumption, a recent study suggested that talin F1 also binds to Rap1 and plays a major role in regulating integrin activation in CHO cells (Gingras et al., 2019). However, the physiological relevance of this interaction and how F0 and F1 are coordinated for Rap1 binding remained unsolved. Besides, interaction of talin with negatively charged membrane lipids (in particular PIP_2) contributes to membrane tethering and activation of talin. Specifically, a helical loop in the F1 domain as well as positively charged patches in the F2 and F3 domains form electrostatic contacts with PIP_2 and stabilize talin at the plasma membrane (Goksoy et al., 2008; Goult et al., 2010; Martel et al., 2001; Saltel et al., 2009).

In this study, we investigated the relative contributions of different talin recruitment and/or activation factors to integrin activity in fibroblasts. Our results emphasize talin as a direct effector of Rap1, which binds to the talin F0 and F1 domains in a cooperative

[1]Max-Planck-Institute of Biochemistry, Department of Molecular Medicine, 82152 Martinsried, Germany. [2]Department of Cardiovascular & Metabolic Sciences, Lerner Research Institute, Cleveland Clinic, 9500 Euclid Ave., Cleveland, OH 44195, USA. [3]Center for Translational Cancer Research (TranslaTUM), TUM School of Medicine, Technische Universität München, 81675 Munich, Germany.
*These authors contributed equally to this work

‡Authors for correspondence (qinj@ccf.org; m.moser@tum.de)

L.Z., 0000-0002-6529-5706; S.K., 0000-0003-4723-056X; M.M., 0000-0001-8825-5566

Received 21 June 2019; Accepted 24 September 2019

manner and synergizes with membrane lipid PIP_2 to recruit and stabilize talin to/at the membrane to regulate integrin activity.

RESULTS AND DISCUSSION

Rap1 synergizes with PIP_2 to regulate talin-mediated integrin activation

To study the relative importance of different talin recruitment factors for integrin regulation, we used a previously established cell culture system of talin1 and talin2 double-deficient fibroblasts (talin$^{1/2dKO}$), that allows reconstitution with wild-type (WT) and mutant talin to analyze integrin activity (Zhu et al., 2017). Cells were retrovirally transduced with constructs encoding C-terminally ypet-tagged talin fusion proteins, which carry mutations in the Rap1-binding site within the F0 domain (K15A/R35A, F0^{DM}) (Bromberger et al., 2018; Zhu et al., 2017), the PIP_2-binding domain in the F2 domain (K272A/K274A) (Song et al., 2012), or RIAM-binding sites in the talin rod domains R3 and R8 (V871Y/V1540Y) (Chang et al., 2014; Yang et al., 2014), as well as combined mutants carrying different combinations of these mutations (Fig. 1A). Cells expressing ypet–talin levels identical to endogenous talin protein levels of control cells (talin1$^{fl/fl}$/talin2$^{-/-}$), were sorted and used for experiments (Fig. 1B,C). Note that all cell groups showed comparable surface integrin levels (Fig. 1C). We performed adhesion assays on the integrin ligands fibronectin (FN) and laminin-111. As expected, talin$^{1/2dKO}$ cells expressing ypet alone as a control hardly adhered to both ligands (Fig. 1D,E). Consistent with our previous study, Rap1-binding-deficient cells revealed an ∼20% reduction in adhesion to both ligands compared to cells expressing WT talin (Zhu et al., 2017). The PIP_2-binding mutant cells also showed a similar reduction in cell adhesion, confirming the role of PIP_2 in regulating integrin activation and cell adhesion. Interestingly, cells expressing a combined 'Rap1/PIP_2' talin mutant showed further reduced adhesion on laminin-111, whereas loss of RIAM-binding to the talin rod had no impact on cell adhesion (Fig. 1D,E). Next, we plated the cells on FN and followed cell spreading for 2 h. While ypet-transduced talin$^{1/2dKO}$ cells remained roundish and did not spread, all talin variants rescued spreading but to a different extent. Cells expressing Rap1- or PIP_2-binding mutants displayed a significant spreading defect, which was further exacerbated in combined mutants, whereas RIAM-binding mutants spread normally as cells expressing WT talin (Fig. 1F). Next, we wondered whether the reduced cell adhesion and spreading of Rap1- and PIP_2-binding deficient cells are caused by impaired focal adhesion formation or integrin activation due to reduced talin recruitment. To this end, we seeded the cells on FN and investigated the formation of focal adhesions by quantification of paxillin-positive areas. Our measurements showed that the focal adhesion (FA) area per cell, the recruitment of talin to FAs (calculated by the ypet fluorescence intensity within FAs in correlation to the total cellular ypet fluorescence intensity), and the amount of active β1 integrins within FAs (determined by staining with antibody clone 9EG7) were significantly reduced in Rap1- and PIP_2-binding mutants compared to WT talin controls, whereas none of these parameters were affected in RIAM-binding mutants (Fig. 1G–I). Overall, these data indicate that Rap1 and PIP_2 act synergistically on talin membrane recruitment to regulate integrin activation, cell adhesion and spreading, while the interaction of the talin rod with RIAM is dispensable for these processes.

The F1 domain of talin harbors a second Rap1-binding site

Both talin F0 and F1 domains form similar ubiquitin-like folds (Goult et al., 2010). Notably, the basic residues in the F0 domain, which form critical contacts with Rap1 in *Dictyostelium*, *Drosophila* and mice (Bromberger et al., 2018; Camp et al., 2018; Plak et al., 2016; Zhu et al., 2017), are also conserved within the talin F1 domain (Fig. 2A). Although we did not detect an obvious interaction between Rap1 and a construct composed of the talin F1 and F2 domains (talin F1F2) in our previous study (Zhu et al., 2017), a recent study showed that Rap1 induced minor chemical shift changes of ^{15}N-labeled talin F1 (Gingras et al., 2019). To clarify this, we first compared the binding of talin F0 and F1 domains to Rap1 using heteronuclear single quantum coherence spectroscopy (HSQC). At relatively low Rap1 concentration (90 µM, molar ratio between Rap1 and talin F0 or F1 is 2:1), the talin F0 domain showed effective binding to Rap1 but interaction between talin F1 and Rap1 was barely detectable (Fig. 2B,C), which was consistent with our previous observation (Zhu et al., 2017). However, an interaction became detectable when we used higher molar ratios between Rap1 and talin F1 domain (5:1). The addition of Rap1 induced chemical shift changes of multiple talin F1 residues but the overall spectral change of talin F1 was much smaller than that of talin F0 under the same conditions (Fig. 2D,E), suggesting a weaker affinity of Rap1 to talin F1 than to talin F0 domain. Indeed, HSQC-based competition experiments revealed a K_i of talin F1 of 1.06 mM, which is three times weaker than that of talin F0 (K_i=0.35 mM) (Fig. 2F). By contrast, the interaction is indeed specific, as double mutations in talin F1 (K98A, R118A; F1^{DM}) that mimic those of talin F0 (K15A, R35A; F0^{DM}) abolished Rap1 binding (Fig. 2G). Like the F0 domain, talin F1 also binds Rap1 in a GTP-dependent manner, as evidenced in Fig. 2H showing that Rap1 loaded with GDP induced smaller chemical shift changes of ^{15}N-labeled talin F1 than active Rap1 loaded with GMP–PNP.

Since the talin head domain adopts a linear conformation where the F1 is sandwiched between the F0 and F2 domains, which may affect the binding of talin F1 domain to Rap1 (Elliott et al., 2010), we performed additional HSQC experiments. Fig. S1A,B clearly shows that the talin F0–Rap1 interaction is dominant at low concentration as the interaction between Rap1 and a construct composed of talin F0^{DM} and the F1 domains (talin F0^{DMF1}) was predominantly blocked. Consistently, talin F0^{DM}F1 only interacts with Rap1 at high concentration, in a manner similar to the isolated F1 domain (Fig. S1C). The similar observation applied also to talin F1F2 (Fig. S1D,E). Taken together, these data suggest that the flanking F0 and F2 domains have negligible effects on the talin F1–Rap1 interaction, which is significantly weaker than the talin F0–Rap1 interaction.

Rap1-binding at talin F0 and F1 domains acts synergistically on integrin activation

Next, we wondered whether the weak talin F1–Rap1 interaction also regulates talin-mediated integrin activity. We first generated C-terminally GFP-tagged talin head domain expression constructs carrying mutations in the F0 (TH-F0^{DM}), the F1 (TH-F1^{DM}) or in both domains (TH-F0^{DM}F1^{DM}) (Fig. 3A) and transfected them into αIIbβ3 integrin-expressing CHO-A5 cells to measure integrin activity using a conformation-specific anti-active human αIIbβ3 integrin (clone PAC1) antibody. Both TH-F0^{DM} and TH-F1^{DM} showed reduced integrin activation levels compared to WT control, however; cells expressing the F1 mutant showed a stronger defect despite the lower affinity of the F1 domain for Rap1 (Fig. 3B). Of note, the combined mutants showed no further reduction in integrin activation. These data are partially in line with the recent study from Gingras et al. (2019). To solve the discrepancies between the CHO cell-based assays and our previous studies in fibroblasts and mice

Journal of Cell Science (2019) 132, jcs235531. doi:10.1242/jcs.235531

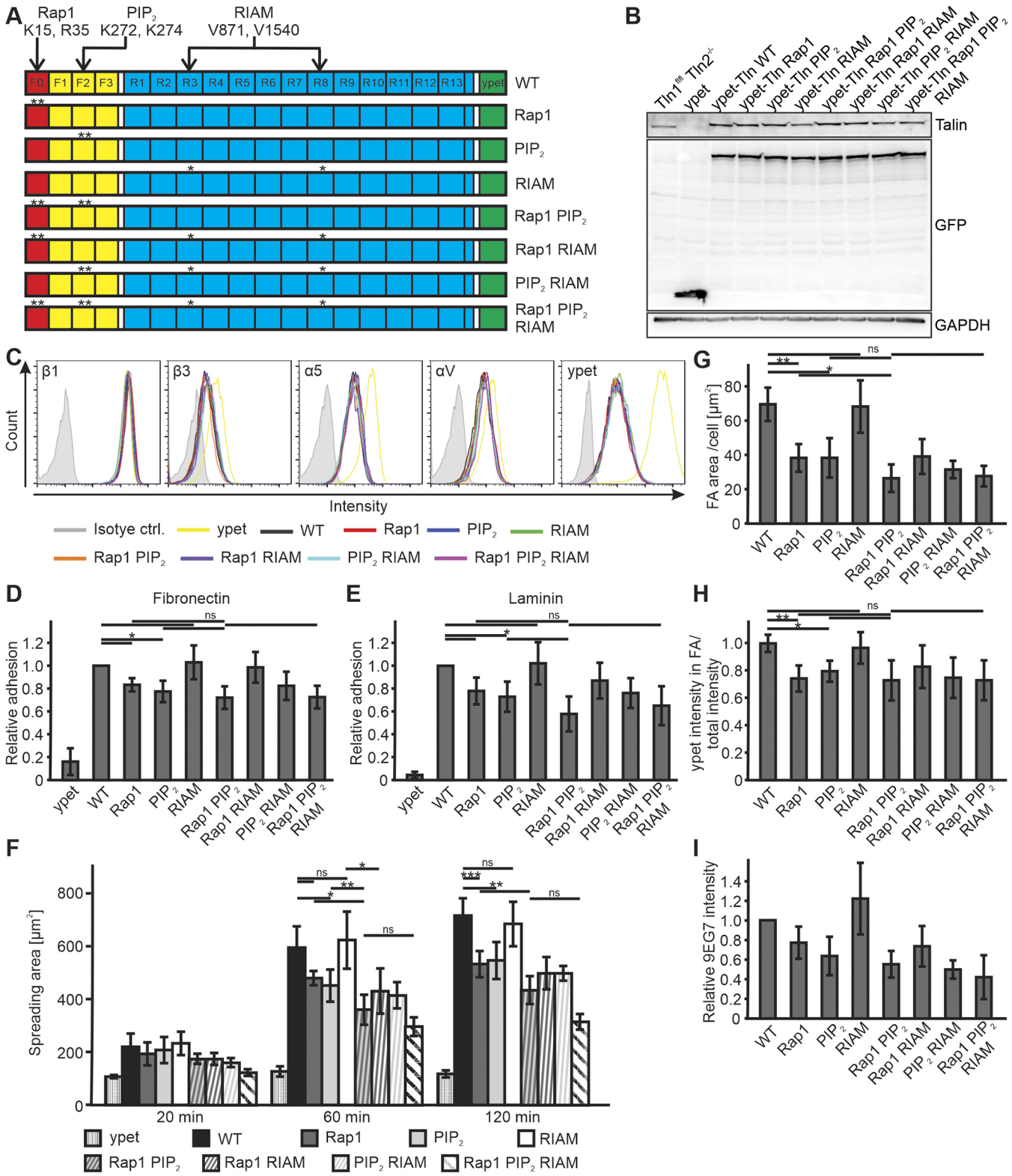

Fig. 1. Rap1 and PIP_2 binding to talin regulate integrin activity in fibroblasts. (A) Schematic overview of ypet-tagged talin variants for re-expression in talin$^{1/2dKO}$ fibroblasts. (B) Expression levels of talin variants assessed by western blotting. (C) FACS analysis of β1, β3, α5 and αV integrin surface levels and ypet intensity. (D,E) Relative adhesion of talin$^{1/2dKO}$ fibroblasts expressing ypet alone or ypet-tagged talin variants carrying the indicated mutations on fibronectin (D) and laminin (E) normalized to unspecific adhesion to poly-L-lysine. Values for cells expressing WT talin were set to 1 (n=8). (F) Spreading area of cells plated on fibronectin for 20, 60 and 120 min (n=6). (G–I) Quantitative analysis of immunofluorescence images of talin$^{1/2dKO}$ fibroblasts expressing various talin variants shown as focal adhesion area (G), ypet intensity in paxillin-positive areas relative to total cellular intensity (H) and intensity of anti-β1 integrin 9EG7 antibody signal within adhesion sites (I) (n=6). Data are presented as mean±95% CI. *P<0.05; **P<0.01; ***P<0.001; ns, not significant by one-way ANOVA followed by Sidak's multiple comparison test.

Journal of Cell Science (2019) 132, jcs235531. doi:10.1242/jcs.235531

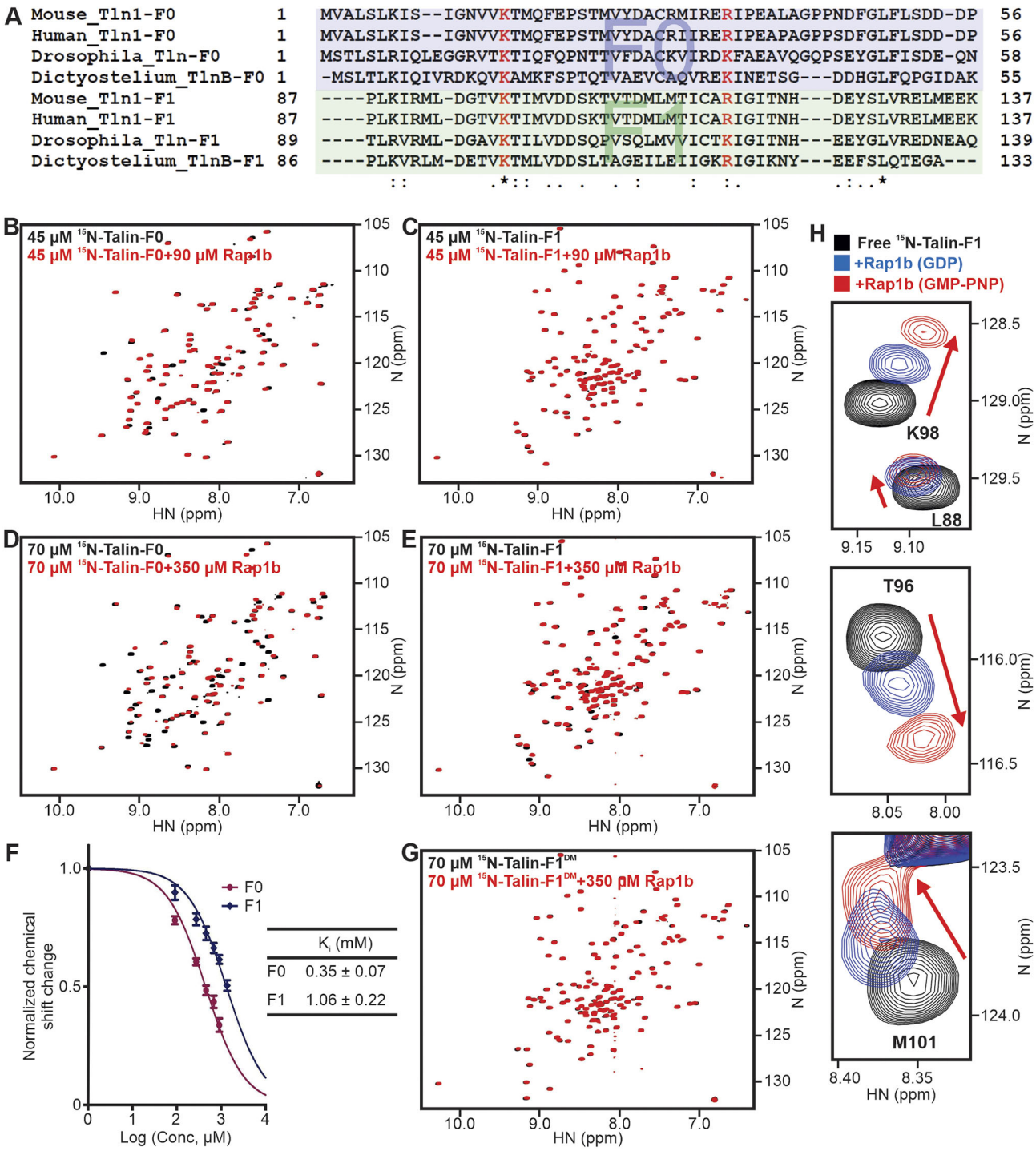

Fig. 2. Rap1 interacts with both talin F0 and F1 domains in a GTP-dependent manner. (A) Excerpt from the protein sequence alignment of mouse, human, *Drosophila* and *Dictyostelium* talin F0 and F1 domains. Conserved positively charged amino acids, corresponding to K15 and R35 in the murine talin F0 domain, are highlighted in red. '*', ':' and '.' indicate conserved, highly and weakly similar residues, respectively. (B–E) HSQC spectra of 45 μM ^{15}N-labeled talin F0 (B) and 45 μM ^{15}N-labeled talin F1 (C) in the absence (black) and presence of 90 μM GMP-PNP-loaded Rap1b (red), and 70 μM ^{15}N-labeled-talin F0 (D) and 70 μM ^{15}N-labeled-talin F1 (E) in the absence (black) and presence of 350 μM GMP-PNP-loaded Rap1b (red). (F) HSQC-based competition experiment to compare the binding of Rap1 to talin F0 and F1. Data are presented as mean±95% CI. (G) HSQC spectra of 70 μM ^{15}N-labeled talin F1^{DM} (K98A, R118A) in the absence (black) and presence of 350 μM GMP-PNP-loaded Rap1b (red). (H) HSQC spectra (residues L88, K98, T96 and M101) of 70 μM ^{15}N-labeled talin F1 in the absence (black) and presence of 350 μM GDP-loaded Rap1b (blue) or GMP-PNP loaded Rap1b (red).

(Zhu et al., 2017; Bromberger et al., 2018), we tested the relative importance of both Rap1-binding sites in our fibroblast system where full-length talin is expressed at physiological levels. Ypet-tagged full-length talin expression constructs carrying Rap1-binding site mutations in the F0 (F0^{DM}), the F1 (F1^{DM}) or in both domains (F0^{DM}F1^{DM}), as well as talin constructs lacking the F0 domain in combination with WT or mutant F1 domains (ΔF0 and ΔF0F1^{DM}) were retrovirally transduced into talin$^{1/2dKO}$ fibroblasts

Journal of Cell Science (2019) 132, jcs235531. doi:10.1242/jcs.235531

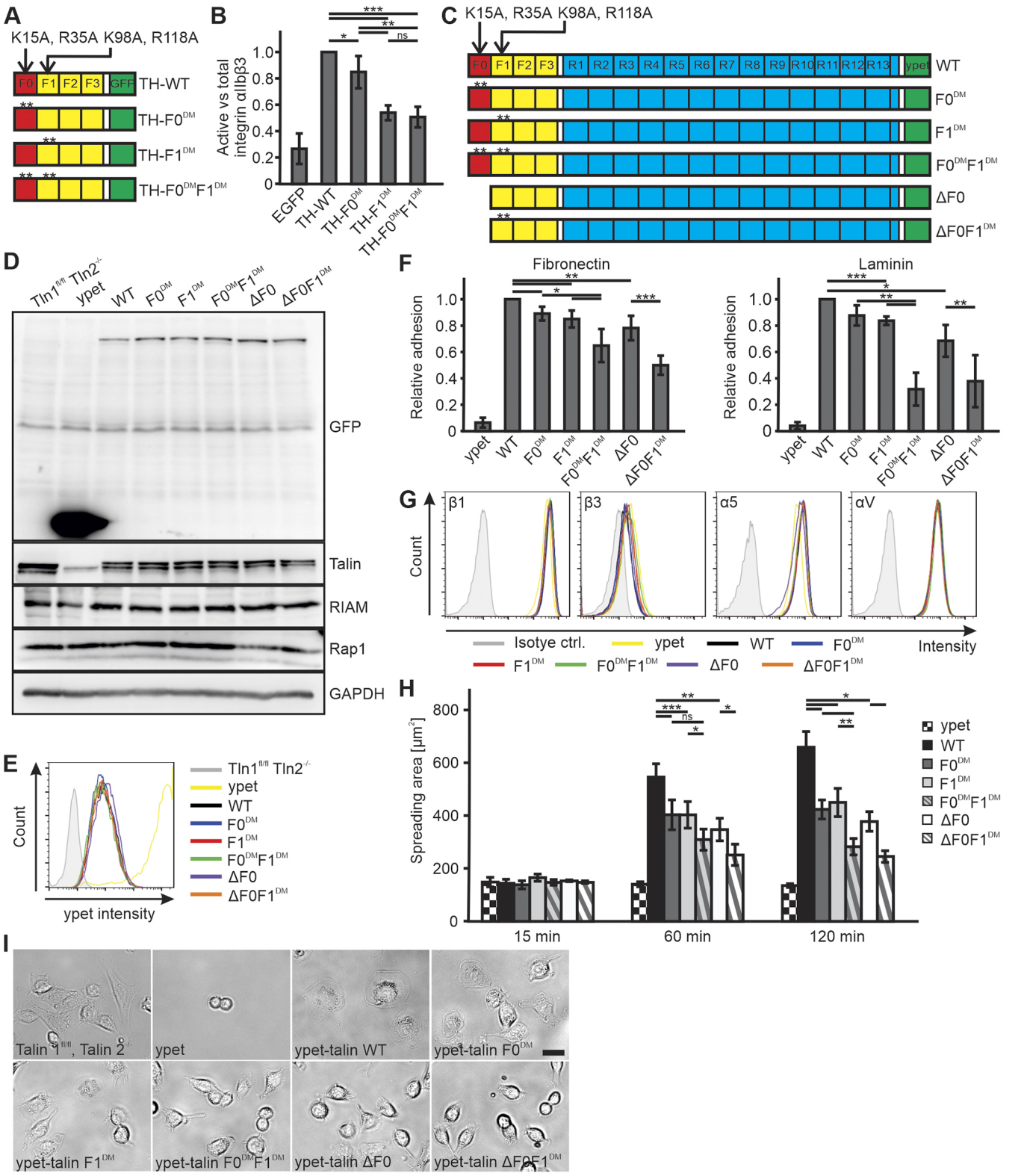

Fig. 3. Binding of Rap1 to talin F0 and F1 domains synergize to promote cell adhesion and spreading. (A) Overview of C-terminally EGFP-tagged talin head (TH) constructs. (B) αIIbβ3 integrin activation in CHO A5 cells expressing EGFP alone or EGFP-tagged TH variants assessed by FACS analysis of clone PAC1 antibody binding. Values were normalized to αIIb integrin surface levels. WT values were set to 1. *n*=5. (C) Schematic overview of ypet-tagged talin variants re-expressed in talin$^{1/2dKO}$ fibroblasts by retroviral transduction. (D) Western blot analyses of ypet-tagged talin variant-transduced cells for their expression of talin, RIAM and Rap1. (E) FACS analysis of ypet intensity in transduced cell lines. (F) Static adhesion of talin$^{1/2dKO}$ fibroblasts expressing ypet, ypet-tagged WT talin or variants on fibronectin and laminin. Values of WT talin-transduced cells were set to 1 (*n*=12/6). (G) FACS analysis of β1, β3, α5 and αV integrin surface levels in talin variant-transduced cells. (H) Spreading area of talin$^{1/2dKO}$ fibroblasts expressing ypet, ypet-talin WT and ypet-talin variants (*n*=6). (I) Phase contrast images of talin1$^{fl/fl}$/talin2$^{-/-}$ cells and talin$^{1/2dKO}$ cells expressing talin variants. Scale bar: 25 µm. Data are presented as mean±95% CI. **P*<0.05; ***P*<0.01; ****P*<0.001; ns, not significant by one-way ANOVA followed by Tukey's (PAC assay shown in B) or Sidak's (adhesion and spreading assays shown in F and H) multiple comparison tests.

and sorted for ypet levels that were identical to talin expression levels of control cells (Fig. 3C-E). Western blot analysis revealed normal Rap1 and RIAM expression in all groups (Fig. 3D). First, we performed cell adhesion assays on FN and laminin-111 and found that adhesion of $F1^{DM}$ cells to both integrin ligands was reduced by a similar level as in $F0^{DM}$ and ΔF0 cells. Importantly, both double $F0^{DM}F1^{DM}$ and $\Delta F0F1^{DM}$ mutants showed a further significant reduction in cell adhesion, indicating an additive effect (Fig. 3F). These alterations were not caused by changes in integrin surface expression levels (Fig. 3G). In line with impaired cell adhesion, $F0^{DM}$, $F1^{DM}$ or ΔF0 cells showed a comparable spreading defect, which was further exacerbated in $F0^{DM}F1^{DM}$ and $\Delta F0F1^{DM}$ cells (Fig. 3H), where the spreading defects persisted and were visible in permanent cultures (Fig. 3I).

Furthermore, immunofluorescence staining (Fig. 4A) revealed that both FA area and number were strongly decreased in $F0^{DM}$ and $F1^{DM}$ cells and were even more dramatically reduced in combined mutant $F0^{DM}F1^{DM}$ cells (Fig. 4B,C). Since most $\Delta F0F1^{DM}$ cells formed very low numbers of apparent FAs, we excluded cells that express talin mutants lacking the F0 domain from these analyses. Similarly, the recruitment of talin to paxillin-positive FAs was reduced to similar levels in $F0^{DM}$ and $F1^{DM}$ cells but was further diminished in $F0^{DM}F1^{DM}$ cells (Fig. 4D). The same observation also applied to β1 integrin activity (relative 9EG7:total β1 integrin fluorescence intensity) within the adhesion sites (Fig. 4E). Taken together, these data strongly suggest that the two Rap1-binding sites act in a synergistic manner in regulating talin membrane recruitment, integrin activation and signaling, which significantly differs from the previous report (Gingras et al., 2019).

Although our study clearly shows that mutations in talin F0 and F1 domains block direct binding of Rap1, we cannot fully exclude that the mutations may affect binding of other Rap1-like small GTPases that additionally contribute to the integrin defects. To address this point, $talin^{1/2dKO}$ fibroblasts expressing WT and talin $F0^{DM}$, $F1^{DM}$ or $F0^{DM}F1^{DM}$ mutants were transfected with mCherry-tagged dominant-negative Rap1 (Rap1DN) or control plasmid. Cells were then plated on fibronectin for 1 h and the spreading areas were determined. Our data revealed that expression of Rap1DN strongly reduced spreading of WT, $F0^{DM}$ and $F1^{DM}$ cells to a similar level as observed in $F0^{DM}F1^{DM}$ cells, but had little effect on spreading of Rap1-binding-deficient $F0^{DM}F1^{DM}$ cells. These data suggest that talin-mediated integrin signaling is highly dependent on Rap1 (Fig. S2). Biochemically, we directly tested the small GTPases Rac1, Cdc42, RhoA and H-Ras, which are known for their roles in integrin signaling, for their interaction with the talin F0 and F1 domains by nuclear magnetic resonance (NMR) HSQC but found no obvious interaction for Rac1, Cdc42 or RhoA (Fig. S3A–F). Interestingly, while being highly homologous to Rap1, H-Ras barely interacted with talin F0 even at high concentration (Fig. S3G), but induced similar chemical shift changes of talin F1 as Rap1 did (Fig. S3H). Moreover, the chemical shift changes were also blocked by the double mutations in the talin F1 domain (Fig. S3I). Together with Fig. S3J,K, our data suggest that F0 is more selective than F1 in binding Rap1 GTPase, and H-Ras binding to F1 may play a compensatory or additive role to Rap1. This may explain the stronger defect of integrin activation caused by the F1 compared to the F0 talin head mutant in the overexpression-based CHO cell assay. More detailed investigations will be required to address this possibility in the future. Nonetheless, all evidence by us and others (Stefanini et al., 2018; Wynne et al., 2012) suggests that Rap1 is the major physiological GTPase involved in integrin activation.

In summary, our study provides a comprehensive analysis of how multiple factors cooperatively regulate talin-mediated integrin signaling.

First, while Rap1 and PIP_2 have been independently shown to be talin regulators (Han et al., 2006; Martel et al., 2001; Saltel et al., 2009), we showed here that Rap1 and PIP_2 synergize to promote potent integrin activation. We note that although only residues on talin F2 that interact with PIP_2 were studied, it is conceivable that additional contacts including a basic helical loop within the F1 domain and positively charged patches in the F3 domain, which both form electrostatic interactions with negatively charged membrane lipids, will further stabilize talin–membrane interactions (Elliott et al., 2010; Goult et al., 2010). These additional interactions are expected to contribute to the talin effect on integrin activation, which explains the modest synergistic effect of our Rap1/ PIP_2 mutants. In contrast, the interaction of RIAM with the talin rod is dispensable for talin recruitment and integrin activity regulation in fibroblasts, which is consistent with the restricted function of RIAM in regulating leukocyte integrin activity (Klapproth et al., 2015; Stritt et al., 2015; Su et al., 2015). Although we cannot exclude the possibility that RIAM binding to the talin F3 domain is involved in talin activation (Yang et al., 2014), RIAM clearly plays a negligible role in talin membrane recruitment in the system we employed here.

Second, we have carefully characterized a second but weaker Rap1-binding site within the talin F1 domain, which shows a similar binding mode as the F0 domain. In a recent study, Gingras et al. (2019) used a CHO cell-based system and claimed that Rap1-binding to only F1 regulates integrin activation. They, thereby, supported their previous report, which suggested that the F0 domain does not contribute to Rap1-mediated integrin activation (Lagarrigue et al., 2018). By using the same assay but a different mutation - i.e. one that causes a stronger defect in Rap1 binding - than the one inserted by Lagarrigue et al. (2018), we did observe an integrin activation defect in F0 mutant cells, which was less strong compared to that in F1 mutant cells. However, data from this *in vitro* assay require careful interpretation as it relies on overexpression of an integrin, which is normally not expressed in this cell line, and a truncated talin lacking the regulatory rod domain. As mentioned above, the stronger defect caused by the F1 mutant in this CHO cell system could be simply due to the disruption of both Rap1 and H-Ras binding to talin F1. In sharp contrast, we employed a more physiological model system to show that interactions of both talin F0 and F1 domains with Rap1 are equally important and they cooperate to regulate talin membrane recruitment and integrin activity. Given that mice with deficient talin F0–Rap1 interaction showed mild phenotypes (Bromberger et al., 2018), it will be interesting to see whether the lower affinity interaction between Rap1 and talin F1 is also of physiological relevance *in vivo* and to what extent both Rap1 binding sites can compensate each other in a mutant mouse model.

How do the interactions of talin F0 and F1 domains with two Rap1 molecules cooperate during integrin activation? We previously observed that the direct interaction between Rap1 and full-length talin or the talin head domain at relatively low concentration resembles the talin F0–Rap1 interaction (Zhu et al., 2017). Together with our findings shown here that talin F1 binds more weakly than talin F0 to Rap1, we propose that talin F0 domain is likely to form initial contact with Rap1 to regulate talin membrane recruitment. This increases the chance of talin F1 binding to another Rap1. The two membrane-bridged Rap1s in Rap1-enriched microdomains would bind talin F0 and F1 with much higher affinity than talin F0 or talin

Journal of Cell Science (2019) 132, jcs235531. doi:10.1242/jcs.235531

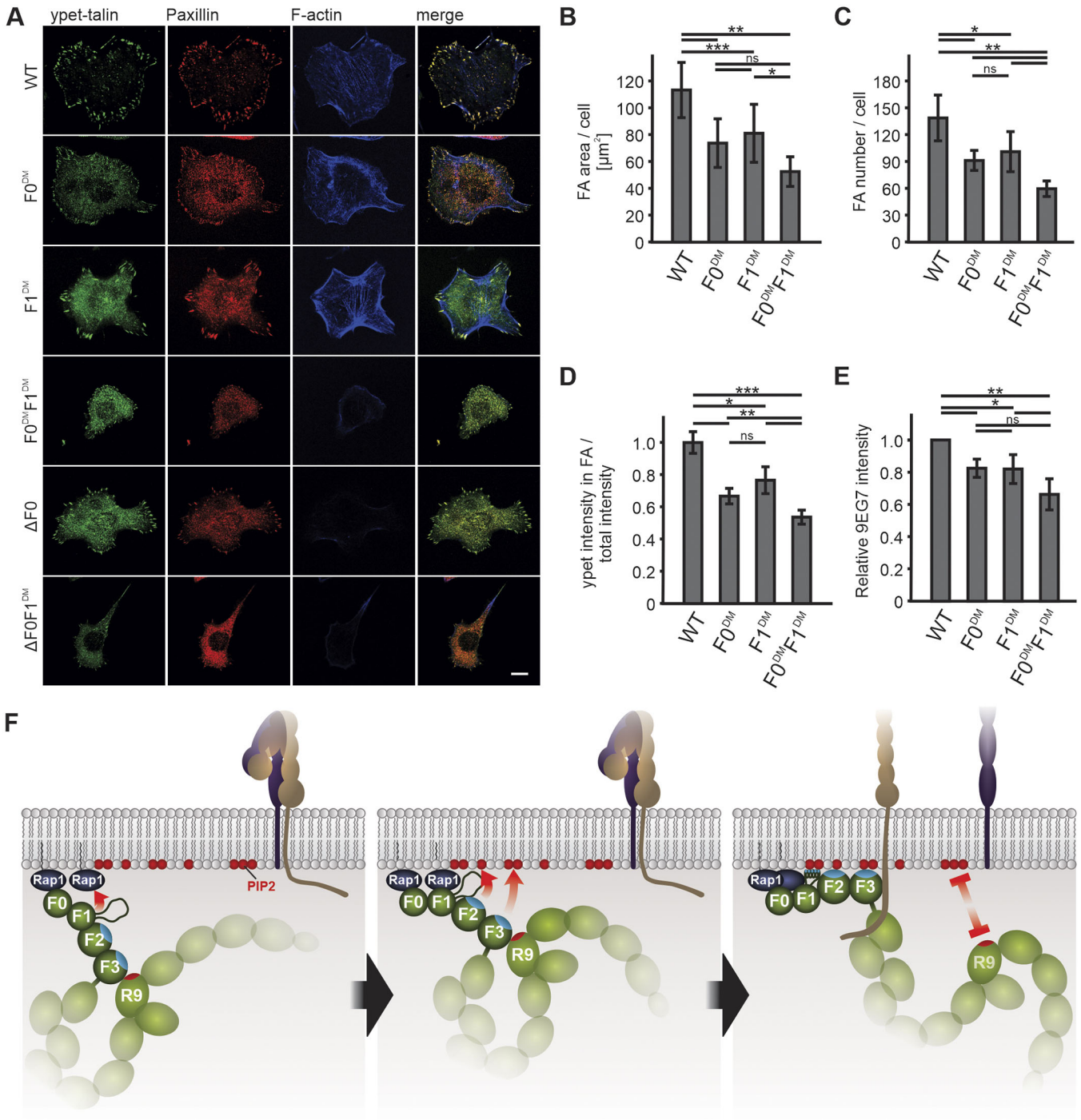

Fig. 4. Rap1 interactions with talin F0 and F1 domains facilitate talin recruitment and regulate integrin activity. (A) Confocal images of talin$^{1/2dKO}$ cells transduced with ypet-talin WT or indicated mutants (green) plated on fibronectin and stained for paxillin (red) and F-actin (blue). Scale bar: 10 µm. (B–E) In fibroblasts expressing ypet-tagged WT talin or ypet-talin variants, focal adhesion area (B) and number per cell (C) were measured (n=6). (D) ypet intensities measured within paxillin-positive areas were normalized to total cellular ypet fluorescence (n=6). (E) Ratio of active (clone 9EG7 staining) to total β1 staining intensities within focal adhesions (n=6). Eight cells were analyzed per experiment and genotype. Data are presented as mean±95% CI. *P<0.05; **P<0.01; ***P<0.001; ns, not significant by one-way ANOVA followed by Tukey's multiple comparison test. (F) Schematic illustration of the proposed model suggesting that talin1 (depicted in green) is recruited to adhesion sites by interaction with the small GTPase Rap1 via both binding sites in its F0 and F1 domain. Rap1 recruits talin to the membrane favorably via the talin F0 domain and further stabilizes the talin head domain at the membrane site by binding to the F1 domain and synergizing with PIP_2–talin F1(loop)F2F3 interaction to trigger integrin activation and cell adhesion.

F1 alone, leading to a synergistic effect in talin membrane recruitment. Membrane tethering of talin is further strengthened by the presence of PIP_2, which leads to strong talin activation, talin–integrin interaction and subsequent integrin activation (Fig. 4F). Consistent with such a targeted recruitment mechanism of talin to Rap1-enriched microdomains, talin was found to be directly recruited to, but not laterally diffuse at, the membrane before it reaches the adhesion sites (Rossier et al., 2012).

Journal of Cell Science (2019) 132, jcs235531. doi:10.1242/jcs.235531

MATERIALS AND METHODS

Cell culture and cell line generation

Talin1 and talin2 double knock-out (talin$^{1/2dKO}$) cells (Theodosiou et al., 2016) were cultured and infected using the Phönix cell system (Austen et al., 2013, 2015) as described earlier (Zhu et al., 2017). Briefly, talin$^{1/2dKO}$ fibroblasts were retrovirally transduced with pLPCX expression constructs containing either ypet alone or C-terminally ypet-tagged murine talin1 cDNA variants: WT talin1, Rap1- (K15A, R35A), PIP_2- (K272A, K274A), or RIAM- (V871Y, V1540Y) binding-deficient single mutants, and double or triple mutant combinations accordingly for one set of experiments. For the second set of experiments, variants unable to bind Rap1 by the F0 domain (F0^{DM}; K15A, R35A), F1 domain (F1^{DM}; K98A, R118A) or both (F0^{DM}F1^{DM}; K15A, R35A, K98A, R118A), as well as mutants lacking the whole F0 domain with intact (ΔF0) or mutant (ΔF0F1^{DM}) F1 Rap1-binding site were used. Cells were FACS-sorted to equal ypet intensity using a FACSAria IIu cell sorter (BD Biosciences).

Talin$^{1/2dKO}$ cells expressing the various talin mutants were transfected with pmCherry-C1 or pmCherry-C1 Rap1aDN (dominant-negative S17N Rap1a mutant) using Lipofectamine 2000 (Thermo Fisher Scientific) following the manufacturer's protocol.

Generated cell lines were characterized by means of western blot following standard protocols. The following antibodies were used: mouse anti-GFP (in-house), mouse anti-talin (Sigma-Aldrich, T3287; 1:20,000), rabbit anti-RIAM (Abcam, 76090; 1:1000), rabbit anti-Rap1 (Santa Cruz Biotechnology, sc-65; 1:500), mouse anti-GAPDH (Merck Millipore, CB1001; 1:20,000), goat anti-mouse-HRP and goat anti-rabbit-HRP (Jackson ImmunoResearch Laboratories, 115-035-003 and 111-035-003; 1:15,000). Surface levels of relevant integrins were determined by FACS analysis using an LSRFortessa X-20 flow cytometer (BD Biosciences) as described earlier (Zhu et al., 2017). The following antibodies were used at a dilution of 1:200: Alexa Fluor 647 hamster IgM isotype control, Alexa Fluor 647 hamster anti-rat CD29, Alexa Fluor 647 hamster anti-mouse CD61, Alexa Fluor 647 rat anti-mouse CD49e and biotin rat anti-mouse CD51 (all BD Biosciences; 562110, 562153, 563523, 564312 and 551380), followed by Cy5-labeled streptavidin (Jackson ImmunoResearch Laboratories, 016-170-084; 1:500). FACS data were analyzed using FlowJo software.

All cells were cultured in DMEM GlutaMAX supplemented with 10% fetal bovine serum, 100 U ml^{-1} penicillin, 100 µg ml^{-1} streptomycin, 2 mM L-glutamine and non-essential amino acids (all from Thermo Fisher Scientific) under standard conditions.

PAC1 integrin activation assay

Wild-type talin head (amino acids 1–405) domain, talin head F0^{DM}, F1^{DM} and F0^{DM}F1^{DM} constructs were cloned into a pEGFP-N1 vector. CHO A5 cells, which express αIIbβ3 integrin (kind gift from Dr David Calderwood, Yale School of Medicine, New Haven, CT), were transiently transfected with empty pEGFP-N1 vector or indicated talin head constructs using Lipofectamine 2000. Integrin activation assays were performed one day after transfection. Briefly, cells were trypsinized and resuspended in Tyrode's buffer (136 mM NaCl, 0.43 mM NaH_2PO_4, 2.7 mM KCl, 12 mM $NaHCO_3$, 5 mM HEPES, 0.1% glucose, 0.35% BSA; pH 7.35) supplemented with 2 mM $CaCl_2$ and 1 mM $MgCl_2$. Cells were incubated with 0.4 mg ml^{-1} RGDS peptide (Sigma-Aldrich) as negative control or left untreated for 10 min and subsequently incubated with Alexa Fluor 647 pre-labeled mouse anti-active human αIIbβ3 antibody (clone PAC1, Thermo Fisher Scientific, MA5-28523; 1:50) for 30 min at room temperature. The PAC1 antibody was labeled using an Alexa Fluor 647 Antibody Labeling Kit (Thermo Fisher Scientific) following the manufacturer's protocol prior to the experiments and stored at 4°C until use. After washing, cells were analyzed using an LSRFortessa X-20 flow cytometer. To assess total levels of αIIb integrin, cells were stained with mouse anti-human CD41a (BD Biosciences, 555465; 1:200) or mouse IgG isotype control (eBioscience, 13-4714-85; 1:200) antibodies, and subsequently with donkey anti-mouse Alexa Fluor 647 antibody (Thermo Fisher Scientific, A31571; 1:200). To calculate integrin activation, the mean fluorescence intensity (MFI) of PAC1 that binds to RGDS-treated cells was substracted from the MFI of PAC1 that binds to untreated cells and divided by the isotype control-corrected MFI of total αIIb integrin $[(MFI_{untreated}-MFI_{RGDS})/(MFI_{\alpha IIb}-MFI_{isotype\ ctrl})]$. Values obtained for cells transfected with WT talin head were set to 1.

Adhesion and spreading assays

Adhesion and spreading assays were performed as described earlier (Zhu et al., 2017). Polystyrol flat-bottom 96-well microplates (Greiner Bio-One) were coated with 10 µg ml^{-1} laminin, 5 µg ml^{-1} fibronectin or 0.01% poly-L-lysine (both Sigma-Aldrich) in coating buffer (20mM Tris-HCl pH 9.0, 150mM NaCl, 2mM $MgCl_2$) overnight at 4°C for adhesion assays. After blocking with 3% BSA/PBS, 2.5×10^4 cells were seeded per well in adhesion medium (DMEM containing 0.1% fetal bovine serum). Plates were washed with PBS after 1 h incubation and adherent cells subsequently fixed with 4% paraformaldehyde and stained with 5 mg/ml Crystal Violet in 2% ethanol. After washing, remaining cell-bound dye was solved in 2% SDS and absorbance was measured at 595 nm using a microplate reader (Tecan). Quadruplets were measured for all groups in each experiment. Results for fibronectin and laminin were normalized to values for poly-L-lysine.

Cell spreading areas were assessed 15, 60 and 120 min after plating the cells on fibronectin-coated dishes (5 µg ml^{-1} in coating buffer, overnight at 4°C). An EVOS FL Auto life cell microscope (Thermo Fisher Scientific) was used to take phase contrast pictures. Spreading area of 20 cells per group was measured in each experiment using ImageJ software (US National Institutes of Health).

Immunostaining and confocal microscopy

Number and area of focal adhesions, talin recruitment and level of active β1 integrin were assessed by immunofluorescence microscopy as previously described (Bromberger et al., 2018; Zhu et al., 2017). Cells were cultured on fibronectin-coated glass coverslips (Thermo Fisher Scientific) for 4 h and either fixed immediately or incubated with rat anti-active β1 integrin antibody (clone 9EG7, BD Biosciences, 553715; 1:100 in PBS) for 30 min on ice and subsequently fixed with 4% paraformaldehyde. Cells were further stained with mouse anti-paxillin (BD Transduction, 610051; 1:300) and phalloidin-conjugated Alexa Fluor 647 (Thermo Fisher Scientific, A22287; 1:100) or, if pre-incubated with 9EG7 antibody, rabbit anti-total β1 integrin (in-house, described in Azimifar et al., 2012; 1:5000). The following secondary antibodies were used: goat anti-mouse Alexa Fluor 546, goat anti-rat Alexa Fluor 546 and goat anti-rabbit Alexa Fluor 647 (all Thermo Fisher Scientific, A11003, A11081 and A21244; 1:300). Images were acquired using a Leica TCS SP5 X confocal microscope (Leica Microsystems) equipped with a 63× NA 1.4 oil objective and processed with Photoshop (Adobe Systems). Quantitative image analyses were carried out with ImageJ software.

Protein purification

The following constructs for bacterial expression were used in this study: mouse talin1-F0 domain (amino acids 1–86), talin1-F1 (83–202), talin1-F0F1 (1–206) and talin1-F1F2 (83–309) subcloned into pHis-1 vectors, and human Rap1b, human Rap1b (G12V) and human H-Ras (G12V) subcloned into pET28a vectors (Zhu et al., 2017). Human RhoA (1–193, Q63L) and Cdc42 (2–178, Q61L) subcloned into pET28a vectors, and human Rac-1 (2–192, Q61L) subcloned into a pET19b vector were kind gifts from Dr Matthias Buck at Case Western Reserve University, Cleveland, OH, USA. Construct mutagenesis was conducted by using QuikChange Lightning site-directed mutagenesis kit (Agilent Technologies). Mutated constructs generated in this study include talin1-F1_DM (K98A, R118A) and talin1-F0F1_DM (K15A, R35A). Each talin fragment was expressed in *E. coli* BL21 (DE3) strain, and ^{15}N isotope-labeled talin fragment expression was achieved by growing bacteria in minimal medium with $^{15}NH_4Cl$ as the sole nitrogen source. Protein was purified using a nickel affinity column and then incubated with TEV protease to remove the recombinant N-terminal 6×His-tag. Untagged protein was collected by means of flow through the nickel affinity column, and then subjected to gel filtration by using Superdex-75 (10/300 or 16/60, GE Healthcare), which was pre-equilibrated with buffer containing 20 mM NaH_2PO_4/Na_2HPO_4 (pH 6.6), 50 mM NaCl and 2 mM dithiothreitol (DTT). Protein concentration was determined by measuring absorbance at 280 nm. All GTPases including Rap1b, Rap1b (G12V), H-Ras (G12V), Rac-1, RhoA and Cdc42 with N-terminal 6×His tag were purified by nickel affinity column, followed by gel filtration using Superdex-75 (16/60, GE Healthcare). Purified wild-type Rap1b was loaded with guanosine 5′-[β-thio] diphosphate trilithium salt (GDP-β-S, Sigma-Aldrich) and all other mutant GTPases were loaded with guanosine

5′-[β, γ-imido] triphosphate trisodium salt (GMP-PNP, Sigma-Aldrich) for experimental use. Protein concentrations of all GTPases were measured using Pierce 660 nm protein assay reagent (Thermo Fisher Scientific).

Nuclear magnetic resonance spectroscopy

2D-HSQC experiments were performed on a Bruker 600 MHz NMR spectrometer. Samples containing ^{15}N-labeled talin fragment (WT or mutant) in the absence or presence of GDP-β-S or GMP-PNP loaded GTPases were studied. Experiments were performed at 25°C in buffer containing 20 mM NaH_2PO_4/Na_2HPO_4 (pH 6.6), 50 mM NaCl, 5 mM $MgCl_2$, 2 mM dithiothreitol (DTT) and 5% D_2O. For HSQC-based competition experiment, increasing amounts of unlabeled talin F0 or talin F1 were mixed with 45 µM ^{15}N-labeled talin F0 in the presence of 90 µM GMP-PNP-loaded Rap1b (G12V). Chemical shift changes of five selected residues (S9, I10, N12, K15, M17) of ^{15}N-labeled talin F0 were calculated. Chemical shift change ($\Delta\delta_{obs\ [HN,N]}$) of each residue was calculated with the equation $\Delta\delta_{obs\ [HN,N]}=[(\Delta\delta_{HN}W_{HN})^2+(\Delta\delta_N W_N)^2)]^{1/2}$ where $\Delta\delta$ (ppm)$=\delta_{bound}-\delta_{free}$, and W_{HN} and W_N are weighting factors, $W_{HN}=1$, $W_N=0.154$. Chemical shift change of each residue was normalized to that observed in the initial sample containing only 45 µM ^{15}N-labeled talin F0 and 90 µM GMP-PNP-loaded Rap1b (G12V). The K_i was fitted by using 'One site – Fit K_i' mode in GraphPad Prism.

Protein sequence analyses

Sequences were aligned using the Clustal Omega multiple sequence alignment tool (Madeira et al., 2019).

Statistical analysis

All data are presented as mean±95% confidence interval (CI). Prism 6 (GraphPad Software) was used for statistical analysis. The given sample size *n* represents the number of independent experiments. Differences between groups were considered statistically significant if $P<0.05$. The degree of significance is indicated as follows in figures: *$P<0.05$, **$P<0.01$, ***$P<0.001$. One-way ANOVA followed by a Tukey's multiple comparison test was carried out to test for overall statistical significance, when each experimental condition was compared to every other condition. In cases in which only selected conditions were compared, one-way ANOVA followed by a Sidak's multiple comparison test was performed.

Acknowledgements

We thank Reinhard Fässler (Max-Planck-Institute of Biochemistry, Martinsried, Germany) for providing us with talin1/2 double knockout fibroblasts.

Competing interests

The authors declare no competing or financial interests.

Author contributions

Conceptualization: J.Q., M.M.; Formal analysis: T.B., L.Z., S.K.; Investigation: T.B., L.Z., S.K.; Writing - original draft: J.Q., M.M.; Writing - review & editing: T.B., L.Z., S.K.; Visualization: T.B., L.Z.; Supervision: J.Q., M.M.; Funding acquisition: J.Q., M.M.

Funding

This work was supported by the National Institutes of Health (NIH P01HL073311 to J.Q.), the Max-Planck-Gesellschaft and the Deutsche Forschungsgemeinschaft (SFB914 TP A01 to M.M.). Deposited in PMC for release after 12 months.

Supplementary information

Supplementary information available online at
http://jcs.biologists.org/lookup/doi/10.1242/jcs.235531.supplemental

References

Austen, K., Kluger, C., Freikamp, A., Chrostek-Grashoff, A. and Grashoff, C. (2013). Generation and analysis of biosensors to measure mechanical forces within cells. *Methods Mol. Biol.* **1066**, 169-184. doi:10.1007/978-1-62703-604-7_15

Austen, K., Ringer, P., Mehlich, A., Chrostek-Grashoff, A., Kluger, C., Klingner, C., Sabass, B., Zent, R., Rief, M. and Grashoff, C. (2015). Extracellular rigidity sensing by talin isoform-specific mechanical linkages. *Nat. Cell Biol.* **17**, 1597-1606. doi:10.1038/ncb3268

Azimifar, S. B., Bottcher, R. T., Zanivan, S., Grashoff, C., Kruger, M., Legate, K. R., Mann, M. and Fassler, R. (2012). Induction of membrane circular dorsal ruffles requires co-signalling of integrin-ILK-complex and EGF receptor. *J. Cell Sci.* **125**, 435-448. doi:10.1242/jcs.091652

Banno, A., Goult, B. T., Lee, H., Bate, N., Critchley, D. R. and Ginsberg, M. H. (2012). Subcellular localization of talin is regulated by inter-domain interactions. *J. Biol. Chem.* **287**, 13799-13812. doi:10.1074/jbc.M112.341214

Bos, J. L. (2005). Linking Rap to cell adhesion. *Curr. Opin. Cell Biol.* **17**, 123-128. doi:10.1016/j.ceb.2005.02.009

Bromberger, T., Klapproth, S., Rohwedder, I., Zhu, L., Mittmann, L., Reichel, C. A., Sperandio, M., Qin, J. and Moser, M. (2018). Direct Rap1/Talin1 interaction regulates platelet and neutrophil integrin activity in mice. *Blood* **132**, 2754-2762. doi:10.1182/blood-2018-04-846766

Brown, N. H., Gregory, S. L., Rickoll, W. L., Fessler, L. I., Prout, M., White, R. A. and Fristrom, J. W. (2002). Talin is essential for integrin function in Drosophila. *Dev. Cell* **3**, 569-579. doi:10.1016/S1534-5807(02)00290-3

Calderwood, D. A., Campbell, I. D. and Critchley, D. R. (2013). Talins and kindlins: partners in integrin-mediated adhesion. *Nat. Rev. Mol. Cell Biol.* **14**, 503-517. doi:10.1038/nrm3624

Camp, D., Haage, A., Solianova, V., Castle, W. M., Xu, Q. A., Lostchuck, E., Goult, B. T. and Tanentzapf, G. (2018). Direct binding of Talin to Rap1 is required for cell-ECM adhesion in Drosophila. *J. Cell Sci.* **131**, Jcs225144. doi:10.1242/jcs.225144

Caron, E., Self, A. J. and Hall, A. (2000). The GTPase Rap1 controls functional activation of macrophage integrin alphaMbeta2 by LPS and other inflammatory mediators. *Curr. Biol.* **10**, 974-978. doi:10.1016/S0960-9822(00)00641-2

Chang, Y. C., Zhang, H., Franco-Barraza, J., Brennan, M. L., Patel, T., Cukierman, E. and Wu, J. (2014). Structural and mechanistic insights into the recruitment of talin by RIAM in integrin signaling. *Structure* **22**, 1810-1820. doi:10.1016/j.str.2014.09.020

Elliott, P. R., Goult, B. T., Kopp, P. M., Bate, N., Grossmann, J. G., Roberts, G. C., Critchley, D. R. and Barsukov, I. L. (2010). The structure of the talin head reveals a novel extended conformation of the FERM domain. *Structure* **18**, 1289-1299. doi:10.1016/j.str.2010.07.011

Gingras, A. R., Lagarrigue, F., Cuevas, M. N., Valadez, A. J., Zorovich, M., Mclaughlin, W., Lopez-Ramirez, M. A., Seban, N., Ley, K., Kiosses, W. B. et al. (2019). Rap1 binding and a lipid-dependent helix in talin F1 domain promote integrin activation in tandem. *J. Cell Biol.* **218**, 1799-1809. doi:10.1083/jcb.201810061

Goksoy, E., Ma, Y. Q., Wang, X., Kong, X., Perera, D., Plow, E. F. and Qin, J. (2008). Structural basis for the autoinhibition of talin in regulating integrin activation. *Mol. Cell* **31**, 124-133. doi:10.1016/j.molcel.2008.06.011

Goult, B. T., Bate, N., Anthis, N. J., Wegener, K. L., Gingras, A. R., Patel, B., Barsukov, I. L., Campbell, I. D., Roberts, G. C. and Critchley, D. R. (2009). The structure of an interdomain complex that regulates talin activity. *J. Biol. Chem.* **284**, 15097-15106. doi:10.1074/jbc.M900078200

Goult, B. T., Bouaouina, M., Elliott, P. R., Bate, N., Patel, B., Gingras, A. R., Grossmann, J. G., Roberts, G. C., Calderwood, D. A., Critchley, D. R. and et al. (2010). Structure of a double ubiquitin-like domain in the talin head: a role in integrin activation. *EMBO J.* **29**, 1069-1080. doi:10.1038/emboj.2010.4

Goult, B. T., Xu, X. P., Gingras, A. R., Swift, M., Patel, B., Bate, N., Kopp, P. M., Barsukov, I. L., Critchley, D. R., Volkmann, N. et al. (2013). Structural studies on full-length talin1 reveal a compact auto-inhibited dimer: implications for talin activation. *J. Struct. Biol.* **184**, 21-32. doi:10.1016/j.jsb.2013.05.014

Han, J., Lim, C. J., Watanabe, N., Soriani, A., Ratnikov, B., Calderwood, D. A., Puzon-Mclaughlin, W., Lafuente, E. M., Boussiotis, V. A., Shattil, S. J. and et al. (2006). Reconstructing and deconstructing agonist-induced activation of integrin alphaIIbbeta3. *Curr. Biol.* **16**, 1796-1806. doi:10.1016/j.cub.2006.08.035

Katagiri, K., Hattori, M., Minato, N., Irie, S., Takatsu, K. and Kinashi, T. (2000). Rap1 is a potent activation signal for leukocyte function-associated antigen 1 distinct from protein kinase C and phosphatidylinositol-3-OH kinase. *Mol. Cell. Biol.* **20**, 1956-1969. doi:10.1128/MCB.20.6.1956-1969.2000

Klapholz, B. and Brown, N. H. (2017). Talin - the master of integrin adhesions. *J. Cell Sci.* **130**, 2435-2446. doi:10.1242/jcs.190991

Klapproth, S., Sperandio, M., Pinheiro, E. M., Prunster, M., Soehnlein, O., Gertler, F. B., Fassler, R. and Moser, M. (2015). Loss of the Rap1 effector RIAM results in leukocyte adhesion deficiency due to impaired beta2 integrin function in mice. *Blood* **126**, 2704-2712. doi:10.1182/blood-2015-05-647453

Lagarrigue, F., Kim, C. and Ginsberg, M. H. (2016). The Rap1-RIAM-talin axis of integrin activation and blood cell function. *Blood* **128**, 479-487. doi:10.1182/blood-2015-12-638700

Lagarrigue, F., Gingras, A. R., Paul, D. S., Valadez, A. J., Cuevas, M. N., Sun, H., Lopez-Ramirez, M. A., Goult, B. T., Shattil, S. J., Bergmeier, W. and Ginsberg, M. H. (2018). Rap1 binding to the talin 1 F0 domain makes a minimal contribution to murine platelet GPIIb-IIIa activation. *Blood Adv* **2**, 2358-2368. doi:10.1182/bloodadvances.2018020487

Lee, H. S., Lim, C. J., Puzon-Mclaughlin, W., Shattil, S. J. and Ginsberg, M. H. (2009). RIAM activates integrins by linking talin to ras GTPase membrane-targeting sequences. *J. Biol. Chem.* **284**, 5119-5127. doi:10.1074/jbc.M807117200

Madeira, F., Park, Y. M., Lee, J., Buso, N., Gur, T., Madhusoodanan, N., Basutkar, P., Tivey, A. R. N., Potter, S. C., Finn, R. D. et al. (2019). The EMBL-

EBI search and sequence analysis tools APIs in 2019. *Nucleic Acids Res.* **47**, 636-641. doi:10.1093/nar/gkz268

Martel, V., Racaud-Sultan, C., Dupe, S., Marie, C., Paulhe, F., Galmiche, A., Block, M. R. and Albiges-Rizo, C. (2001). Conformation, localization, and integrin binding of talin depend on its interaction with phosphoinositides. *J. Biol. Chem.* **276**, 21217-21227. doi:10.1074/jbc.M102373200

Nieswandt, B., Moser, M., Pleines, I., Varga-Szabo, D., Monkley, S., Critchley, D. and Fassler, R. (2007). Loss of talin1 in platelets abrogates integrin activation, platelet aggregation, and thrombus formation in vitro and in vivo. *J. Exp. Med.* **204**, 3113-3118. doi:10.1084/jem.20071827

Plak, K., Pots, H., Van Haastert, P. J. and Kortholt, A. (2016). Direct interaction between TalinB and Rap1 is necessary for adhesion of Dictyostelium cells. *BMC Cell Biol.* **17**, 1. doi:10.1186/s12860-015-0078-0

Reedquist, K. A., Ross, E., Koop, E. A., Wolthuis, R. M., Zwartkruis, F. J., Van Kooyk, Y., Salmon, M., Buckley, C. D. and Bos, J. L. (2000). The small GTPase, Rap1, mediates CD31-induced integrin adhesion. *J. Cell Biol.* **148**, 1151-1158. doi:10.1083/jcb.148.6.1151

Rossier, O., Octeau, V., Sibarita, J. B., Leduc, C., Tessier, B., Nair, D., Gatterdam, V., Destaing, O., Albigès-Rizo, C., Tampé, R. et al. (2012). Integrins beta1 and beta3 exhibit distinct dynamic nanoscale organizations inside focal adhesions. *Nat. Cell Biol.* **14**, 1057-1067. doi:10.1038/ncb2588

Saltel, F., Mortier, E., Hytönen, V. P., Jacquier, M.-C., Zimmermann, P., Vogel, V., Liu, W. and Wehrle-Haller, B. (2009). New PI(4,5)P_2- and membrane proximal integrin-binding motifs in the talin head control beta3-integrin clustering. *J. Cell Biol.* **187**, 715-731. doi:10.1083/jcb.200908134

Sebzda, E., Bracke, M., Tugal, T., Hogg, N. and Cantrell, D. A. (2002). Rap1A positively regulates T cells via integrin activation rather than inhibiting lymphocyte signaling. *Nat. Immunol.* **3**, 251-258. doi:10.1038/ni765

Song, X., Yang, J., Hirbawi, J., Ye, S., Perera, H. D., Goksoy, E., Dwivedi, P., Plow, E. F., Zhang, R. and Qin, J. (2012). A novel membrane-dependent on/off switch mechanism of talin FERM domain at sites of cell adhesion. *Cell Res.* **22**, 1533-1545. doi:10.1038/cr.2012.97

Stefanini, L., Lee, R. H., Paul, D. S., O'shaughnessy, E. C., Ghalloussi, D., Jones, C. I., Boulaftali, Y., Poe, K. O., Piatt, R., Kechele, D. O. et al. (2018). Functional redundancy between RAP1 isoforms in murine platelet production and function. *Blood* **132**, 1951-1962. doi:10.1182/blood-2018-03-838714

Stritt, S., Wolf, K., Lorenz, V., Vogtle, T., Gupta, S., Bosl, M. R. and Nieswandt, B. (2015). Rap1-GTP-interacting adaptor molecule (RIAM) is dispensable for platelet integrin activation and function in mice. *Blood* **125**, 219-222. doi:10.1182/blood-2014-08-597542

Su, W., Wynne, J., Pinheiro, E. M., Strazza, M., Mor, A., Montenont, E., Berger, J., Paul, D. S., Bergmeier, W., Gertler, F. B. and et al. (2015). Rap1 and its effector RIAM are required for lymphocyte trafficking. *Blood* **126**, 2695-2703. doi:10.1182/blood-2015-05-644104

Theodosiou, M., Widmaier, M., Bottcher, R. T., Rognoni, E., Veelders, M., Bharadwaj, M., Lambacher, A., Austen, K., Muller, D. J., Zent, R. et al. (2016). Kindlin-2 cooperates with talin to activate integrins and induces cell spreading by directly binding paxillin. *eLife* **5**, e10130. doi:10.7554/eLife.10130

Wynne, J. P., Wu, J., Su, W., Mor, A., Patsoukis, N., Boussiotis, V. A., Hubbard, S. R. and Philips, M. R. (2012). Rap1-interacting adapter molecule (RIAM) associates with the plasma membrane via a proximity detector. *J Cell Biol* **199**, 317-330. doi:10.1083/jcb.201201157

Yang, J., Zhu, L., Zhang, H., Hirbawi, J., Fukuda, K., Dwivedi, P., Liu, J., Byzova, T., Plow, E. F., Wu, J. et al. (2014). Conformational activation of talin by RIAM triggers integrin-mediated cell adhesion. *Nat. Commun.* **5**, 5880. doi:10.1038/ncomms6880

Zhang, H., Chang, Y. C., Huang, Q., Brennan, M. L. and Wu, J. (2016). Structural and functional analysis of a talin triple-domain module suggests an alternative talin autoinhibitory configuration. *Structure* **24**, 721-729. doi:10.1016/j.str.2016.02.020

Zhu, L., Yang, J., Bromberger, T., Holly, A., Lu, F., Liu, H., Sun, K., Klapproth, S., Hirbawi, J., Byzova, T. V. et al. (2017). Structure of Rap1b bound to talin reveals a pathway for triggering integrin activation. *Nat. Commun.* **8**, 1744. doi:10.1038/s41467-017-01822-8